V European Conference on Computational Fluid Dynamics
ECCOMAS CFD 2010
J. C. F. Pereira and A. Sequeira (Eds)
Lisbon, Portugal,14-17 June 2010

A SIXTH-ORDER COMPACT FINITE-VOLUME SCHEME FOR AEROACOUSTICS: APPLICATION TO A LARGE EDDY SIMULATION OF A JET

Arnaud Fosso Pouangué*, **Hugues Deniau*** and **Nicolas Lamarque***

*CERFACS,
42, Avenue Gaspard Coriolis, Toulouse, France
e-mail: fosso@cerfacs.fr

Key words: Jet, Large Eddy Simulation, Finite-Volume, high-order scheme, Compact Interpolation, Aeroacoustics

Abstract. *Realizing high-fidelity simulations is a key issue in Computational Fluid Dynamics (CFD) for Aeroacoustics (CAA) studies. Indeed, in this case, CFD computations are required both to satisfy the stringent constraints of CAA and to allow a deep insight in the mechanisms responsible for the noise generation. For these purposes, high-order compact schemes are recognized as useful tools to deal with the numerical schemes aspects of this problem. However, while many studies deal with high-order compact schemes in a Finite-Difference (FD) context, just few use Finite-Volume (FV) approaches. In previous works, the authors have developed a compact scheme in a Finite Volume approach. This compact scheme is formulated in the physical space to be suitable to highly irregular meshes and thus be able to handle complex geometries. The purpose of the present work is to demonstrate the capabilities of the scheme by simulating a round jet flow with a Large Eddy Simulation (LES) approach. The configuration considered is a Mach = 0.3 jet of diameter* $D = 5cm$. *The Reynolds of the jet is* $Re_j = 3.21\ 10^5$. *Experimental measurements have been realized at the Laboratoire d'Etudes Aerodynamiques (LEA) of Poitiers, by Laurendeau et al. The nozzle lips have a thickness of* $e = D/100$. *The measured thickness of the mixing layer is around* $\delta_\omega = 0.032D$ *and the potential core ends at about* $4.8D$ *downstream to the nozzle exit. The mixing layer is already turbulent at the nozzle exit but with a weak turbulence rate of 0.4%. The performed computations include the nozzle geometry in order to well reproduce these trends.*

1 INTRODUCTION

In order to serve for aeroacoustics studies, CFD computations are required both to satisfy the stringent constraints of Computational Aeroacoustics (CAA) [1] and to allow a deep insight in the mechanisms responsible for the noise generation. It is now well established that high-order compact schemes are useful tools to deal with the spatial discretization aspects of the issue.

While many studies deal with high-order compact schemes in a Finite-Difference (FD) context, just few use Finite-Volume (FV) approaches. However FV formulations are more popular for industrial applications due to their robustness since they are generally based on a weak formulation of the field equations. Therefore, they require less solution and mesh smoothness than FD methods. Moreover, they are conservative. If the former advantage is not yet valid for high-order FV schemes, the latter still holds true. Among recent studies are the works of [2] and those of [3]. The former authors build high-order FV schemes in the computational domain. A coordinate transformation is then applied between the physical and the computational spaces to keep the high-order accuracy. The latter authors introduce a second-order compact scheme directly in the physical space. Even if this approach is more complex than the previous, it is well suited for highly irregular grids because it removes the error associated with the discrete representation of metric terms.

In line with the works of [3], [4] developed a formally sixth-order compact FV scheme for compressible flows, directly in the physical space. The fluxes are determined by a high-order compact interpolation using cell-averaged quantities. The main difference between this new scheme and the Lacor and coworkers one is the use of a local frame defined using the mesh line as a preferred direction. The method aims to keep the sixth-order in this preferred direction. Specific treatments are also done to deal with multi-block formulation, and the resulting scheme is proved to be theoretically stable. The scheme is implemented in a fully parallel multi-block structured finite-volume code (*elsA* software developed by ONERA and CERFACS). [4] also shows that the resulting scheme has a high-order accuracy and is low dispersive and low dissipative even on highly irregular meshes for academic test cases.

The purpose of the present work is to demonstrate the capabilities of such a scheme by simulating a round jet flow with a Large Eddy Simulation (LES) approach. The configuration considered is a Mach = 0.3 jet of diameter $D = 5$cm. The Reynolds of the jet is $Re_j = 3.21\ 10^5$. Experimental measurements have been realized at the Laboratoire d'Etudes Aerodynamiques (LEA) of Poitiers, by Laurendeau et al. [5]. The simulation of this configuration is a first step towards the simulation of jet noise fluidic control using microjets which was the object of Laurendeau and coauthors work.

The present paper is organised as follows. Section 2 briefly presents the compact scheme developed by [4]. Then, section 3 gives a description of the jet configuration considered and the meshing strategy. Section 4 follows by describing other numerical tools used to perform computations like the time-marching algorithm and the boundary conditions. Then, results are discussed in Section 5. The results given by the compact scheme are also compared to those obtained using a third order Roe solver for convective fluxes, which is a traditionnal solver used in the code.

2 HIGH ORDER FINITE VOLUME SCHEMES

2.1 Presentation of the scheme for linear problems

Let be considered the following linear convection equation:

$$\frac{\partial u}{\partial t} + \nabla \cdot \mathbf{f}(u) = 0, \tag{1}$$

where $\mathbf{f}(u)$ is a linear vectorial function of u. By integrating Eq. (1) over a volume control Ω and using the Stokes formula, one can obtain:

$$V\frac{\mathrm{d}\bar{u}}{\mathrm{d}t} + \oint_{\partial\Omega} \mathbf{f}(u) \cdot \mathbf{n}\mathrm{d}S = 0, \tag{2}$$

with $V = |\Omega|$ and

$$\bar{u} = \frac{1}{V}\int_{\Omega} u\mathrm{d}\Omega.$$

Now, it is assumed that Ω is a polyhedron (polygon in 2D), *i.e.* the unitary normal on each of its faces is constant over the face. Therefore, using the linearity of $\mathbf{f}$, Eq. (2) leads to:

$$V\frac{\mathrm{d}\bar{u}}{\mathrm{d}t} + \sum_{i=1}^{n_f} \mathbf{f}\left(\int_{\partial\Omega_i} u\mathrm{d}S\right) \cdot \mathbf{n}_i = 0, \tag{3}$$

where n_f is the number of faces and $\partial\Omega_i$, the i-th face of Ω. Eq. (3) is equivalent to

$$V\frac{\mathrm{d}\bar{u}}{\mathrm{d}t} + \sum_{i=1}^{n_f} \mathbf{f}\left(\tilde{u}_i\right) S_i \cdot \mathbf{n}_i = 0, \tag{4}$$

where $S_i = |\partial\Omega_i|$ and

$$\tilde{u}_i = \frac{1}{S_i}\int_{\partial\Omega_i} u\mathrm{d}S.$$

Hence, to obtain a high-order discretization of Eq. (4), it is sufficient to have a high-order approximation of the face-averaged quantity $\tilde{u}_i$.

Now, a three-dimensional structured (indexed by (i, j, k)) grid composed of polyhedrons is considered. This section presents the different strategies proposed to approximate at a high-order the interface-averaged value of a quantity u on the interface $(i + 1/2, j, k)$, using cell-averaged values of neighbouring cells. In this section, the mesh line (j, k) for which these two indexes remain constant is under consideration. To make this approximation spatially implicit or compact, the formula involves averaged values on neighbouring interfaces $(i - 1/2, j, k)$ and $(i + 3/2, j, k)$. Thus the compact interpolation reads as

$$\alpha\tilde{u}_{i-1/2,j,k} + \tilde{u}_{i+1/2,j,k} + \beta\tilde{u}_{i+3/2,j,k} = \sum_{l=-m}^{l=n}\sum_{p=-q}^{p=r}\sum_{s=-t}^{s=u} a_{l,p,s}\bar{u}_{i+l,j+p,k+s}, \tag{5}$$

where

$$\bar{u}_{i,j,k} = \frac{1}{V_{i,j,k}} \int_{V_{i,j,k}} u \mathrm{d}V, \tag{6}$$

are cell-averaged values and

$$\tilde{u}_{i+1/2,j,k} \approx \frac{1}{S_{i+1/2,j,k}} \int_{S_{i+1/2,j,k}} u \mathrm{d}S, \tag{7}$$

approximate interface-averaged values. The interpolation coefficients α, β and $a_{l,p,s}$ are chosen, depending on the interface $(i+1/2, j, k)$, in order to obtain a given order of approximation.
The system of equations formed with Eq. (5) along the mesh line (j,k) to compute values at the interfaces is a tridiagonal system. This choice has been made since this system is efficiently inversed using, for example, the Thomas algorithm. Moreover, the inversion of the system could be done for each grid line in each dimension.
To determine the interpolation coefficients, a Taylor series expansion is done for each term in Eq. (5), and two possibilities are studied in this paper depending on the following choice:

- u is considered as a function of s, the curvilinear abscissa along the (j,k) line;
- u is considered as a function in a well chosen tridimensional coordinates system (x', y', z').

Two types of schemes could be derived from these considerations and are discussed in details in [4]. For sake of convenience, only the more general approach using the second consideration is presented here. This approach has been shown to be more efficient in highly irregular meshes on academic test cases however both methods give similar results on smooth grids.
Therefore, u is considered as a function of three coordinates x, y, z for three-dimensionnal flow. Thus a Taylor series expansion introduced in Eq. (5) involves all derivatives with respect to these three directions:

$$u(x,y,z) = \sum_{m=0}^{\infty} \sum_{n=0}^{\infty} \sum_{p=0}^{\infty} \frac{1}{m!} \frac{1}{n!} \frac{1}{p!} (x-x_0)^m (y-y_0)^n (z-z_0)^p \frac{\partial^{m+n+p} u}{\partial x^m \partial y^n \partial z^p} (x_0, y_0, z_0). \tag{8}$$

Remembering that averaged values as defined by Eq. (6) and Eq. (7) are considered, relations obtained using the Taylor series expansion involve kinetic moments $J_{\Omega}^{x^m y^n z^p} = \int_{\Omega} (x - x_{\Omega})^m (y - y_{\Omega})^n (z - z_{\Omega})^p \mathrm{d}\Omega$ of cells and interfaces which belong to the stencil.
The main idea of the scheme consists in the definition of a new frame, local to each interface, in which the Taylor series expansions are performed. Indeed, since only the interfaces $(i-1/2, j, k)$, $(i+1/2, j, k)$ and $(i+3/2, j, k)$ appear in Eq. (5), the proposed scheme has already a preferred direction along this (j,k)-line. Thus a new frame (x', y', z') (see Fig. 1) is introduced so that the x'-direction represents this preferred direction, tangent to (j,k) mesh line. Taylor series expansions are written in this frame, and all derivatives

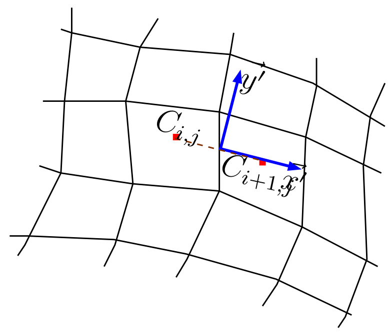

(a) Orthogonal frame defined by the cell centers line.

Figure 1: Different local frames considered for the high-order curvilinear interpolation.

	Derivatives	Total number
1D	$\partial^{(0)}, \partial^{(i)}_{x^i}$, $i = 1, ..., 5$	6
2D	$\partial^{(0)}, \partial^{(i+j)}_{x^i y^j}$, $i, j \in \{0, ..., 5\}$, $i + j \leq 5$	21
3D	$\partial^{(0)}, \partial^{(i+j+k)}_{x^i y^j z^k}$, $i, j, k \in \{0, ..., 5\}$, $i + j + k \leq 5$	56

Table 1: Derivatives to cancel out in order to get a formal sixth-order interpolation in all directions.

along x' are cancelled out in order to get the sixth-order accuracy in this direction.

It would be too expensive to satisfy all transverse derivatives (along y' and z') relations. Indeed, in the two dimensional case for example, there are 15 more relations to satisfy in order to get a sixth-order scheme for transverse derivatives (see Tab. 1) and it would be too expensive to use a suitable stencil to fullfill these relations. Therefore, transverse derivatives are accounted for as corrections terms using a least square approach. The scheme account for all transverse derivatives up to the fourth order ($\partial y'$, $\partial x'y'$, $\partial y'^2$, $\partial x'^2 y'$, $\partial x' y'^2$, and $\partial y'^3$) and use four supplementary cells in 2D case (eight supplementary cells in 3D). The list of all derivatives used are presented in Tab. 2. Fig. 2 presents the resulting stencil in 2D case. The four points represented by a square are used to match the derivatives in x' direction, and the four points represented by a circle ($\bullet$) are used for transversal correction.

To treat multiblock boundaries, an explicit fourth-order formulation is used on the boundary interface ($i = 1/2$):

$$\tilde{u}_{1/2,j,k} = \sum_{l=-1}^{l=2} \sum_{p=-q}^{p=r} \sum_{s=-t}^{s=u} a_{l,p,s} \bar{u}_{l,j+p,k+s}. \quad (9)$$

This scheme allows to keep conservativeness on multiblock boundaries at an acceptable computational cost since no parallel inversion of a tridiagonal system is needed and only two ghost cells are necessary. For stability reasons, an implicit decentered fifth-order

Dimension	Derivatives	Total number
2D	$\partial^{(0)}$, $\partial x'$, $\partial^2 x'^2$, $\partial^3 x'^3$, $\partial^4 x'^4$, $\partial^5 x'^5$, $\partial y'$, $\partial^2 y'^2$, $\partial^2 x'y'$, $\partial^3 y'^3$, $\partial^3 x'^2 y'$, $\partial^3 x' y'^2$	12
3D	$\partial^{(0)}$, $\partial x'$, $\partial^2 x'^2$, $\partial^3 x'^3$, $\partial^4 x'^4$, $\partial^5 x'^5$, $\partial y'$, $\partial z'$, $\partial^2 y'^2$, $\partial^2 z'^2$, $\partial^2 x'y'$, $\partial^2 x'z'$, $\partial^2 y'z'$, $\partial^3 y'^3$, $\partial^3 z'^3$, $\partial^3 x'^2 y'$, $\partial^3 x' y'^2$, $\partial^3 x'^2 z'$, $\partial^3 x' z'^2$, $\partial^3 y'^2 z'$, $\partial^3 y' z'^2$, $\partial^3 x' y' z'$	22

Table 2: Derivatives used for the general curvilinear scheme.

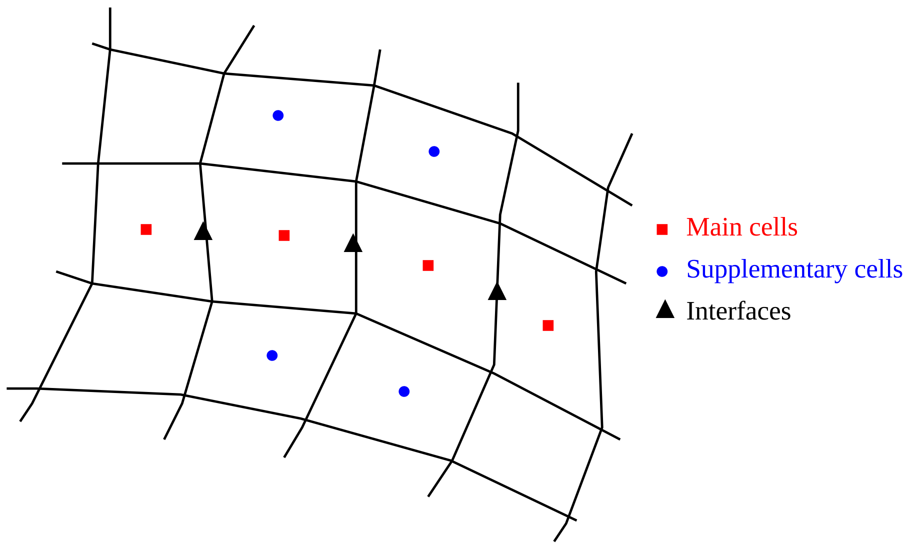

Figure 2: Cells used by the curvilinear interpolation.

scheme is used on the second interface $(i = 3/2)$:

$$\alpha \tilde{u}_{i-1/2,j,k} + \tilde{u}_{i+1/2,j,k} + \beta \tilde{u}_{i+3/2,j,k} = \sum_{l=0}^{l=2} \sum_{p=-q}^{p=r} \sum_{s=-t}^{s=u} a_{l,p,s} \bar{u}_{1+l,j+p,k+s}. \tag{10}$$

So in this latter formula, the ghost cell is not used.

More details about the local frame, the least square approach and the multi-block boundary closures used could be found in [4].

2.2 Discretization of the compressible Navier-Stokes equations

Here are considered the compressible Navier-Stokes equations written in conservative form:

$$\begin{aligned} \frac{\partial W}{\partial t} \quad &+ \frac{\partial E_c}{\partial x} + \frac{\partial F_c}{\partial y} + \frac{\partial G_c}{\partial z} \\ &+ \frac{\partial E_d}{\partial x} + \frac{\partial F_d}{\partial y} + \frac{\partial G_d}{\partial z} \quad = 0, \end{aligned} \tag{11}$$

where

$$W = (\rho, \rho u, \rho v, \rho w, \rho e)^t \,, \tag{12}$$

is the vector of conservative variables,

$$\begin{aligned} E_c &= \Big(\rho u, \rho u^2 + p, \rho uv, \rho uw, (\rho e + p)u\Big)^t \,, \\ F_c &= \Big(\rho v, \rho uv, \rho v^2 + p, \rho vw, (\rho e + p)v\Big)^t \,, \\ G_c &= \Big(\rho w, \rho uw, \rho vw, \rho w^2 + p, (\rho e + p)w\Big)^t \end{aligned}$$

are the convective flux densities,

$$\begin{aligned} E_d &= (0, -\tau_{11}, -\tau_{12}, -\tau_{13}, -(\tau_{11}u + \tau_{12}v + \tau_{13}w) + q_1)^t \,, \\ F_d &= (0, -\tau_{21}, -\tau_{22}, -\tau_{23}, -(\tau_{21}u + \tau_{22}v + \tau_{23}w) + q_2)^t \,, \\ G_d &= (0, -\tau_{31}, -\tau_{32}, -\tau_{33}, -(\tau_{31}u + \tau_{32}v + \tau_{33}w) + q_3)^t \end{aligned}$$

are the diffusive flux densities, p is the pressure, τ the stress constrainsts tensor and q the heat flux vector.

In the present paper, for the convective fluxes, the following formulation is used, for each interface $(i + 1/2, j, k)$:

$$\tilde{\mathcal{F}}_c \approx S(E_c(\tilde{W})\tilde{n}_x + F_c(\tilde{W})\tilde{n}_y + G_c(\tilde{W})\tilde{n}_z). \tag{13}$$

where, $\tilde{\mathcal{F}}_c$ is the convective flux on the interface $(i + 1/2, j, k)$, $\tilde{W}$ is the vector of the $(i + 1/2, j, k)$ interface-averaged values of the conservative variables computed using the above presented compact interpolation. This formulation is formally only second-order accurate, but it has been observed [4] that it could reach at least a fifth-order accuracy using the above presented compact interpolation method if the grid is sufficiently regular. For diffusive fluxes, a traditional second-order method implemented in *elsA* has been used. Indeed, since the convective time scale are much smaller than the diffusive time scale considering the Reynolds of applications focused, this second-order method is sufficient.

3 CONFIGURATION AND MESHING

The configuration considered is a 0.3 mach jet of diameter $D = 5$cm. The Reynolds of the jet is $Re_j = 3.21\ 10^5$. Experimental measurements have been realized at the Laboratoire d'Etudes Aerodynamiques (LEA) of Poitiers, by Laurendeau et al. [5]. The nozzle lips have a thickness of $e = D/100$. The measured thickness of the mix layer is around $\delta_\omega = 0.032D$ and the potential core ends at about $4.8D$ downstream to the nozzle exit accordingly to the experimental measurements. The full nozzle geometry, including walls and lips, are included in the computational domain and meshed.

Meshes are structured and composed with several blocks. The domain is meshed using a H-mesh inside, surrounded by parts of O-meshes to avoid the axis-singularity (see Fig. 3).

In the axial direction, the points are stretched in the nozzle such a way that the axis step size goes from $\Delta x_{phys} = 0.04D$ to $\Delta x_0 = 0.001D$. From of the end of the nozzle to about $8D$ downstream (this zone contains the predicted potential core), the points are stretched in order to reach a spatial step of $\Delta x_{phys} = 0.04D$. Then this step is kept constant until the end of the physical zone of interest at $12D$ downstream the nozzle exit. Then, the step size grows to reach $\Delta x_{sponge} = 0.2D$ at the end of the sponge layer zone at about $25D$ downstream the nozzle exit.
In the radial direction, from the center to the nozzle lips, the points are in a first time equally spaced with a step of $\Delta r_0 = \Delta x_0$ and then stretched to reach a spatial step of $\Delta x_{cis} = \delta_\omega/20$ such a way that there is 20 points in the predicted boundary layer thickness at the nozzle exit. With that refinement, it is possible to put 8 poins on the lips of the nozzle. Then from the nozzle lips to the end of the physical zone of interest at about $6D$ from the nozzle exit, the step size is progressively increased to reach $\Delta r_{phys} = \Delta x_{phys} = 0.04D$. Then the step size is progressively increased to reach $\Delta r_{sponge} = \Delta x_{sponge} = 0.2D$ at the end of the sponge layer zone.
In the azimuthal direction, 185 points are equally distributed so there is at least one point every two degrees.
Finally, the mesh contains about 22 millions of points.
All data are nondimensionalized by the inlet density and sound speed so that $D^+ = 1$, $\rho^+ = 1$, $c^+ = 1$ and $p^+ = 1/\gamma$, where c is the speed of sound and γ is the specific heat ratio.

4 NUMERICAL PROCEDURE

4.1 Spatial schemes

The LES is performed using the curvilinear compact Finite-Volume scheme (CUR6) presented in section 2 and using a third-order Roe solver (ROE 3) already implemented in *elsA* for comparisons. The compact scheme is associated to a compact filter presented further to get stable computations. This filter is also considered as an implicit subgrid-scale model [6]. The ROE 3 computations are used without any subgrid-scale model since an artificial dissipation is already present through the limiter operator.

4.2 Filtering

The filters chosen are compact filters, precisely the sixth-order and eight-order filters proposed by [7] have been used. The inner filter scheme reads:

$$\alpha_f \hat{u}_{i-1} + \hat{u}_i + \alpha_f \hat{u}_{i+1} = \sum_{n=-N}^{N} a_n \bar{u}_{i+n}, \tag{14}$$

where α_f is a parameter ranging from -0.5 to 0.5. The authors also recommend to use high-order one sided formulas on boundaries instead of decreasing the order of the filter. The one-sided formulas are defined by

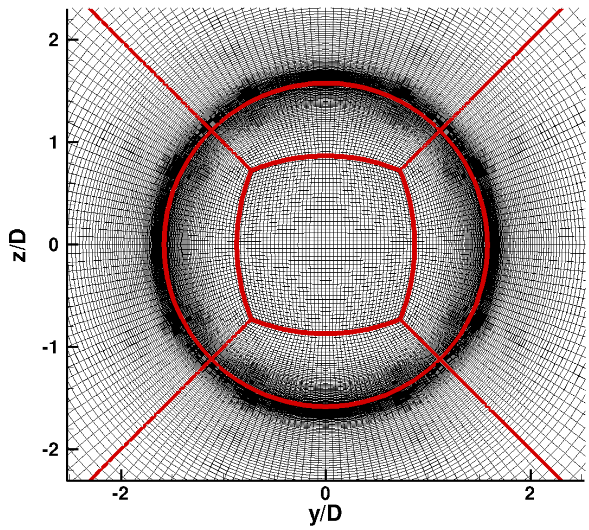

(a) Zoom on the center of the mesh in the (y, z) plane

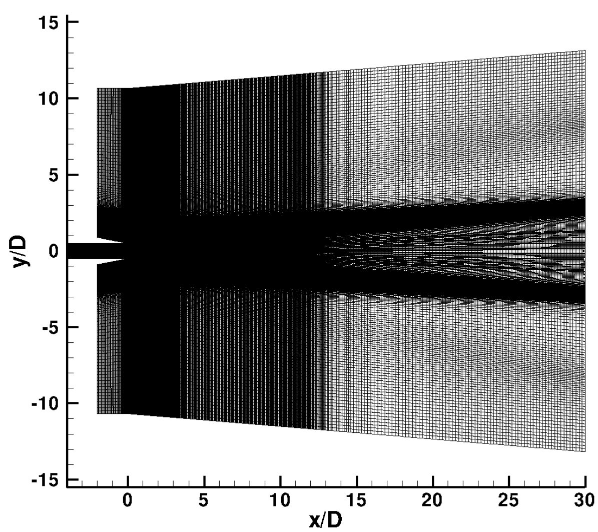

(b) Mesh view in the (x, y) plane

Figure 3: Instantaneous vorticity magnitude near the jet axis and velocity divergence field out of the jet.

$$\begin{aligned} \hat{u}_1 &= \bar{u}_1, & (15) \\ \alpha_f \hat{u}_{i-1} + \hat{u}_i + \alpha_f \hat{u}_{i+1} &= \sum_{n=1}^{2N+1} a_n \bar{u}_n,\ i = 2, ..., N. & (16) \end{aligned}$$

The filtering is applied in the computational plane. In multidimensional case, filtering operator is applied successively in each dimension. One can remark that, in each direction, the first and the last points are not filtered. This could be a drawback since anti-diffusion is possible at this point. Since for multiblock problems two ghost cells are used, the filtering includes these points so that the first unfiltered point is fictitious. The combination of the filtering operator and the compact scheme has been shown to be efficient on academic test cases in [4]. The sixth-order filter is used with a parameter α set to 0.49.

4.3 Time-marching numerical scheme

The time integration scheme used for these computations is the following optimized sixth-steps Runge-Kutta method [8]

$$\left\{ \begin{array}{lcl} u^{(0)} &=& u_n, \\ u^{(k)} &=& u^{(0)} + \alpha_k \Delta t L(u^{(k-1)}), \quad k = 1, ..., 6, \\ u_{n+1} &=& u^{(6)}, \end{array} \right. \tag{17}$$

with L, the space discretization operator and $\alpha_1 = 0.11797990162882$, $\alpha_2 = 0.18464696649448$, $\alpha_3 = 0.24662360430959$, $\alpha_4 = 0.33183954253762$, $\alpha_5 = 0.5$, $\alpha_6 = 1.0$. This scheme is second-order accurate for non-linear problems but is optimized in the wavenumber space.

4.4 Boundary conditions

4.4.1 Inflow

Bogey and Bailly have shown in previous works that it is important not to apply the inflow injection directly at the nozzle exit. Therefore, the inflow injection is applied in the nozzle, at a distance of 4D upstream the nozzle exit. The inflow conditions are applied using the radiative boundary condition of Tam and Webb [9] combined with a sponge zone on the conservative field. This combination has been successfully used by [10] and allow to obtain a very less reflexive inflow condition. The radiative boundary condition is used on a range of 8 points rather than on the boundary only. This range of points is entirely included in the sponge zone layer.

To accelerate the generation of the turbulence at the nozzle exit, perturbations are injected at the nozzle inlet using randomly generated vortex-ring velocity fluctuations.

4.4.2 Outflow and external flow

At the jet outflow, a Navier-Stokes characteristic boundary condition (NSCBC) method using the local one-dimensional inviscid (LODI) approach [11] is used. It is combined with a sponge zone layer which consists in applying a relaxation parameter on pressure. External flow boundaries are computed by application of the radiative boundary condition combined with the same type of sponge zone layer as for the outflow.

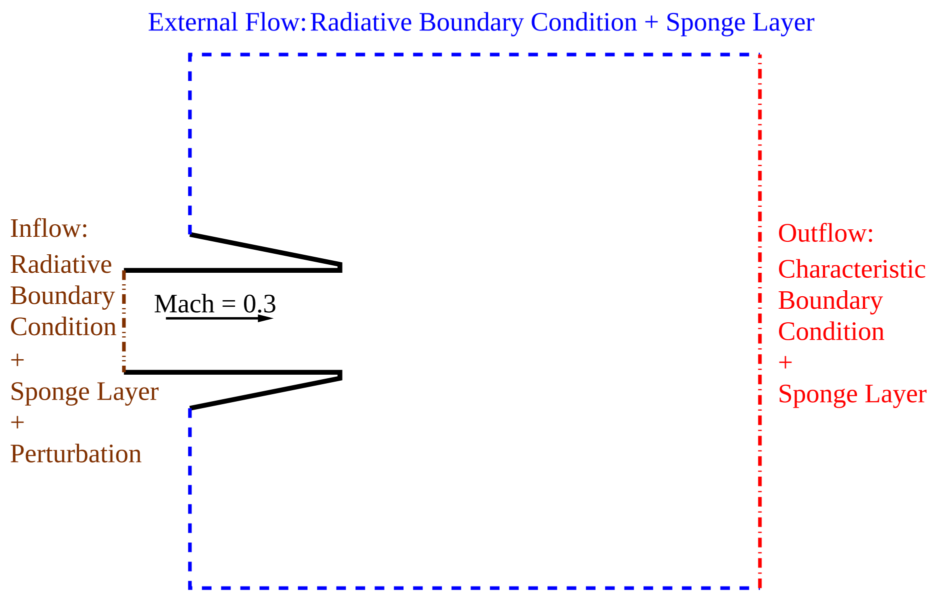

Figure 4: Boundary conditions used for the jet simulation.

5 RESULTS

Simulations have been running for 1.2×10^5 iterations corresponding to about $t = 19D/U_j$. Perturbations have been injected just for the last 4×10^4 iterations. Therefore, it is clear that flow statistics are not converged yet. As a consequence, the mean and rms levels are not presented here.
Fig. 5 shows instantaneous vorticity magnitude near the jet axis and instantaneous velocity divergence out of the jet for both ROE 3 and CUR6 schemes. Looking at these results, it is clear that the third-order Roe solver is too dissipative compared with the compact scheme. First, it is seen on Fig. 5 that vortices are more diffused for the ROE 3 case. After $x = 5D$, there are much more vorticity maxi with the CUR6 scheme than with the ROE 3 scheme. Thus, the CUR6 scheme is able to solve smaller scales and this is confirmed by the velocity divergence field. Indeed, this velocity divergence field highlight the acoustic waves emissed by turbulence. Compared to the CUR 6 velocity divergence field, the ROE 3 velocity divergence field is only composed of the lower frequency waves. For both schemes, the jet mixing layer is destabilized around $x = 0.5D$ as shown in Fig. 6. This is due to the fact that the simulation has not been performed for enough time to get an effective influence of the perturbations injection. Indeed, the perturbations are

expected to excite the higher-order modes and thus destabilize the mixing layer of the jet earlier.

6 CONCLUSIONS

This paper has presented a LES of a round jet using a curvilinear compact scheme in a Finite-Volume approach developed in the physical space. This scheme is implemented in the *elsA* code. The round jet simulated is a Mach=0.3 jet at a Reynolds number of 3.21×10^5. Results obtained are qualitatively compared to those obtained using a third-order Roe scheme which is traditionally used in the *elsA* code. Although computations are not converged as far as statistics are concerned, it is clear that the compact scheme is more suitable to simulate high-Reynolds number. The trends observed also show that the different tools (boundary conditions, sponge layer and perturbations injection) associated to the compact scheme could be an effective building block for aeroacoustics studies. More quantitative results will be available soon.

REFERENCES

[1] C. K. W. Tam, Computational Aeroacoustics: Issues and Methods, AIAA Journal, **33** , 1788–1796 (1995).

[2] M. Piller and E. Stalio, Compact Finite Volume Schemes on Boundary-Fitted Grids, Journal of Computational Physics, **227** , 4736–4762 (2008).

[3] C. Lacor, S. Smirnov and M. Baelmans, A Finite Volume Formulation of Compact Schemes on Arbitrary Structured Grids, Journal of Computational Physics, **198** , 16–42 (2004).

[4] A. Fosso P., H. Deniau, F. Sicot and P. Sagaut, Curvilinear Finite Volume Schemes using High-Order Compact Interpolation, accepted by Journal of Computational Physics (2010).

[5] E. Laurendeau, P. Jordan, J. P. Bonnet, J. Delville, P. Parnaudeau and E. Lamballais, Subsonic jet noise reduction by fluidic control: The interaction region and the global effect, Physics of Fluids, **20** , 101519.1–101519.15 (2008).

[6] C. Bogey and C. Bailly, Decrease of the Effective Reynolds Number With Eddy-Viscosity Subgrid-Scale Modelling, AIAA Journal, **43**(2) , 437–439 (2005).

[7] D. V. Gaitonde and M. R. Visbal, Further Development of a Navier-Stokes Solution Procedure based on Higher-Order formulas, 37th Aerospace Sciences Meeting and Exhibit, Reno, Nevada, **AIAA-1999-557**, (1999).

[8] C. Bogey and C. Bailly, A Family of Low Dispersive and Low Dissipative Explicit Schemes for Flow and Noise Computations, Journal of Computational Physics, **194** , 194–214 (2004).

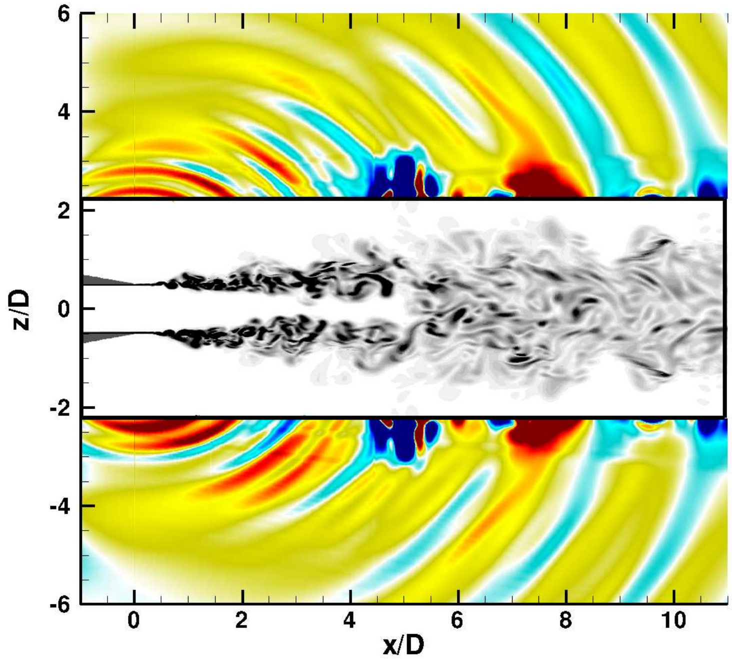

(a) Third Order Roe scheme.

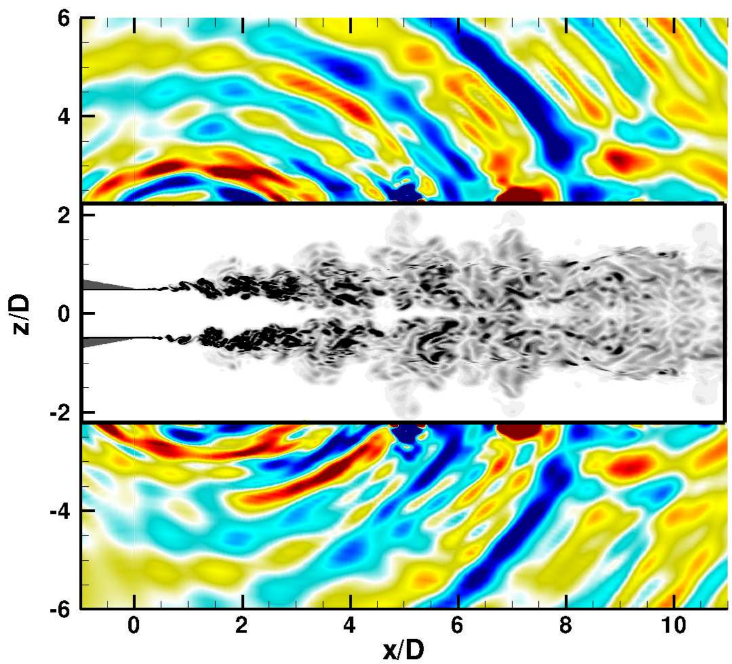

(b) Curvilinear Compact scheme.

Figure 5: Instantaneous vorticity magnitude near the jet axis and velocity divergence field out of the jet.

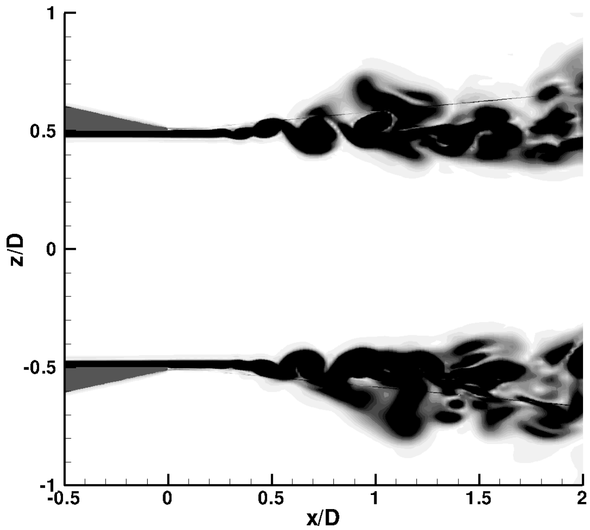

(a) Third Order Roe scheme.

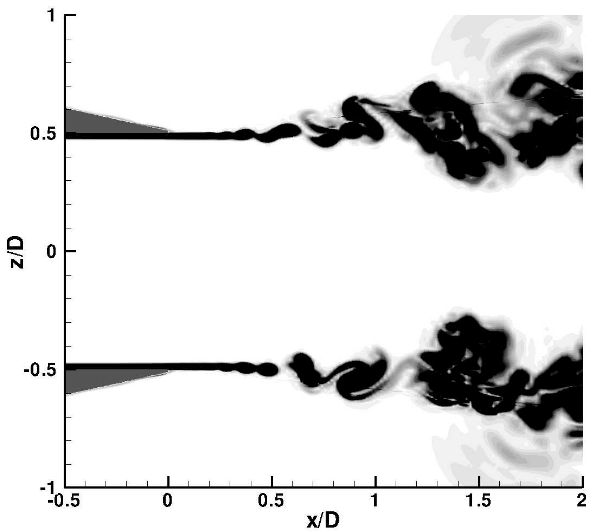

(b) Curvilinear Compact scheme.

Figure 6: Instantaneous vorticity in the center of the jet.

[9] C. K. W. Tam and J. C. Webb, Dispersion-Relation-Preserving Finite Difference Schemes for Computational Acoustics, Journal of Computational Physics, **107** , 262–281 (1993).

[10] C. Bogey, C. Bailly and , Noise Investigation of a High Subsonic, Moderate Reynolds Number Jet Using a Compressible Large Eddy Simulation, Theoretical and Computational Fluid Dynamics, **16** , 273–297 (2003).

[11] T. J. Poinsot and S. K. Lele, Boundary Conditions for Direct Simulations of Compressible Viscous Flows, Journal of Computational Physics, **101** , 104–129 (1992).